JPEDAV (2009) 30:509–516
DOI: 10.1007/s11669-009-9565-3
1547-7037 ©ASM International



# A Semi-Empirical Atomistic Approach in Materials Research

*Byeong-Joo Lee*

*(Submitted March 23, 2009; in revised form May 4, 2009)*

**With developments of semi-empirical interatomic potentials for realistic materials systems, atomistic approaches to a wide range of bulk and nanostructured materials become more and more feasible. This article outlines a recently developed semi-empirical interatomic potential model, the second nearest-neighbor modified embedded-atom method that shows a strong applicability to multicomponent systems. It is shown that the interatomic potentials can well reproduce fundamental physical properties of representative materials systems. Examples are used to illustrate the applications of the atomistic approach to calculation of fundamental physical properties of both nano and bulk structural materials such as thermodynamic, elastic, interface, and defect properties necessary to understand the materials behavior and to serve as input to larger-scale simulations.**

**Keywords** computation, kinetics, Monte Carlo simulations, thermodynamics

## 1. Introduction

With continuously increasing industrial demands for better materials performance, an elaborate control of structural evolution and materials properties becomes highly necessary. An elaborate control of structures and materials properties requires better understanding of the materials behavior from a more fundamental level, e.g., the atomic level. Atomistic simulations (molecular dynamics or Monte Carlo) can be a useful tool to analyze and predict phase transformations kinetics, defects, structural evolutions, and mechanical behaviors of materials. Moreover, fundamental physical quantities such as grain boundary energy, diffusivity, and interactions between defects computed from atomistic simulations can be used as input data for larger-scale simulations.

First-principles (FP) calculations usually deal with less than a thousand atoms, which is insufficient to handle lots of materials phenomena. Using semi-empirical interatomic potentials, the number of atoms in atomistic simulations can be increased by several orders of magnitute. In such simulations, the reliability of the interatomic potential is crucial.

A reliable atomic potential should reproduce various physical properties of an element, such as elastic properties, structural properties, defect properties, surface properties, and thermal properties. Several dozens of interatomic potential models have been published.[1] These models were mostly for a small group of elements. One had to use different formalisms for elements of different crystal structures. It was difficult to describe alloy systems consisting of elements with different structures. In contrast, the modified embedded-atom method (MEAM[2]) potential is highly applicable because it can describe atomic potentials of wide range of elements (fcc, bcc, hcp, diamond, and even gaseous elements) using a common formalism while achieving good agreements with experimental results or FP calculations. The MEAM was created by Baskes,[2] by modifying the EAM[3] so that the directionality of bonding is considered. The original MEAM only considers the interactions among first nearest-neighbor atoms. Recently, the MEAM was modified once again by Lee and Baskes[4,5] such that the interactions among second nearest-neighbor atoms were partially considered and thus some critical shortcomings of the original MEAM were overcome. The generalized MEAM (second nearest neighbor or 2NN MEAM) has been applied to a wide range of elements including bcc,[5] fcc,[6] hcp[7] metals, manganese,[8] diamond structured elements such as carbon,[9] silicon,[10] germanium,[11] gaseous elements (H, N, O),[2] and to binary systems between different types of elements, e.g., Fe-Cu,[12] Fe-Pt,[13] Fe-Ti,[14] Fe-Mn,[8] Ni-W,[15] Fe-C,[16] Fe-N,[17] Fe-H,[18] Ti-C,[19] and Ti-N[19] systems.

The performance of the 2NN MEAM potentials of some elements and alloy systems will be demonstrated by applying them to describe fundamental physical properties of relevant materials. This article will then show the

This article is an invited paper selected from participants of the 14th National Conference and Multilateral Symposium on Phase Diagrams and Materials Design in honor of Prof. Zhanpeng Jin's 70th birthday, held November 3-5, 2008, in Changsha, China. The conference was organized by the Phase Diagrams Committee of the Chinese Physical Society with Drs. Huashan Liu and Libin Liu as the key organizers. Publication in *Journal of Phase Equilibria and Diffusion* was organized by J.-C. Zhao, The Ohio State University; Yong Du, Central South University; and Qing Chen, Thermo-Calc Software AB.

**Byeong-Joo Lee**, Department of Materials Science and Engineering, Pohang University of Science and Technology, Pohang 790-784, Republic of Korea. Contact e-mail: calphad@postech.ac.kr.

applicability of the atomistic approaches based on the 2NN MEAM to provide fundamental physical quantities and to analyze basic materials phenomena.

## 2. Interatomic Potential

In the MEAM, the total energy of a system is given in the following form:

$$E = \sum_i \left[ F_i(\bar{\rho}_i) + \frac{1}{2} \sum_{j(\neq i)} S_{ij} \phi_{ij}(R_{ij}) \right], \quad \text{(Eq 1)}$$

where $F_i$ is the embedding function for an atom $i$ embedded in a background electron density $\bar{\rho}_i$, and $S_{ij}$ and $\phi_{ij}(R_{ij})$ are the screening function and the pair interaction between atoms $i$ and $j$ separated by a distance $R_{ij}$. For energy calculations, the functional forms for $F_i$ and $\phi_{ij}$ should be given. The background electron density at each atomic site is computed by considering the directionality of bonding, that is, by combining several partial electron density terms for different angular contributions with weight factors $t^{(h)}$ ($h$ = 1-3). Each partial electron density is a function of atomic configuration and atomic electron density. The atomic electron densities $\rho^{a(h)}$ ($h$ = 0-4) are given as

$$\rho^{a(h)}(R) = \rho_o \exp[-\beta^{(h)}(R/r_e - 1)], \quad \text{(Eq 2)}$$

where $\rho_o$ is the atomic electron density scaling factor and $\beta^{(h)}$ is the decay lengths are adjustable parameters, and $r_e$ is the nearest-neighbor distance in the equilibrium reference structure. A specific form is given to the embedding function $F_i$, but not to the pair interaction $\phi_{ij}$. Instead, a reference structure where individual atoms are on the exact lattice points is defined and the total energy per atom of the reference structure is estimated from the zero-temperature universal equation of state developed by Rose et al.[20] Then, the value of the pair interaction is evaluated from the known values of the total energy per atom and the embedding energy, as a function of the nearest-neighbor distance. In the original MEAM,[2] only first nearest-neighbor interactions are considered. The neglect of the second and higher nearest-neighbor interactions is made effective by the use of a strong many-body screening function.[21] The consideration of the second nearest-neighbor interactions in the modified formalism is implemented by adjusting the screening parameters, $C_{min}$, so that the many-body screening becomes less severe. In addition, a radial cutoff function[21] is applied to reduce the calculation time. Details of the (2NN) MEAM formalism have been published in the literature[2,4-7] and will not be repeated here. Some calculated physical properties of Al and Fe are presented in Table 1, in comparison with available experimental data.

Most of the properties listed in Table 1 are 0 K properties. It is shown that thermal properties are also correctly reproduced. The calculated temperature dependence of bulk modulus shows a good agreement with experimental data,[22-26] as illustrated in Fig. 1. The composition dependences of various fundamental properties in alloy systems are also correctly reproduced. As an example, the lattice parameter, cohesive energy, and bulk modulus of various stable and unstable compounds in the Ni-W binary system are compared with experimental or FP data in Table 2.

**Table 1 Calculated physical properties of Al and Fe using 2NN MEAM potentials,[5,6] in comparison with experimental data**

| Property | MEAM-Al (exp.) | MEAM-Fe (exp.) |
|---|---|---|
| $C_{11}$, $10^{12}$ dyne/cm$^2$ | 1.143 (1.143) | 2.430 (2.431) |
| $C_{12}$, $10^{12}$ dyne/cm$^2$ | 0.619 (0.619) | 1.380 (1.381) |
| $C_{44}$, $10^{12}$ dyne/cm$^2$ | 0.316 (0.316) | 1.219 (1.219) |
| $E_v^f$, eV | 0.68 (0.68) | 1.75 (1.79) |
| $Q^D$, eV | 1.33 (1.33) | 2.28 (2.5) |
| $E_I^f$, eV | 2.49 (–) | 4.20 (–) |
| $E_{(100)}$, mJ/m$^2$ | 848 (1085(a)) | 2510 (2360(a)) |
| $E_{(110)}$, mJ/m$^2$ | 948 (1085(a)) | 2356 (2360(a)) |
| $E_{(111)}$, mJ/m$^2$ | 629 (1085(a)) | 2668 (2360(a)) |
| $\Delta d_{(100)}$, % | +1.8 (+1.8) | −1.1 (−0.2, −1.5) |
| $\Delta d_{(110)}$, % | −8.9 (−8.5 ± 1.0) | −1.5 (0) |
| $\Delta d_{(111)}$, % | +1.0 (0.9 ± 0.5) | −10.5 (−16.9) |
| $\Delta E_{bcc/fcc}$, eV/atom | 0.12 (0.10(b)) | 0.048 (0.082(b)) |
| $\Delta E_{fcc/hcp}$, eV/atom | 0.03 (0.06(b)) | −0.018 (−0.023(b)) |
| ε(0-100 °C), $10^{-6}$/K | 22.0 (23.5) | 12.4 (12.1) |
| $C_p$ (0-100 °C), J/mol·K | 26.2 (24.7) | 26.1 (25.5) |
| m.p., K | 937 (933) | 2000 (1811) |
| $\Delta H_m$, kJ/mol | 11.0 (10.7) | 13.2 (13.8) |
| $\Delta V_m$, % | 6.7 (6.5) | 4.0 (3.5) |

Values listed are the elastic constants $C_{11}$, $C_{12}$, $C_{44}$, the relaxed vacancy formation energy $E_v^f$, the activation energy of vacancy diffusion $Q^D$, the relaxed formation energy of self interstitial $E_I^f$, the (100), (110), and (111) surface energy $E_{(100)}$, $E_{(110)}$, and $E_{(111)}$ and surface relaxation $\Delta d$, the structural energy differences $\Delta E$, thermal expansion coefficient ε, specific heat $C_p$, melting point m.p, enthalpy change $\Delta H_m$, and volume change $\Delta V_m$ due to melting.

(a) Average value for polycrystal

(b) Thermodynamically assessed values (room temperature data)

## 3. Atomistic Computation of Physical Properties

In this section, it is demonstrated that some physical properties which are difficult to measure experimentally can be computed rather efficiently using the atomistic approach. The properties include interfacial energy, grain boundary diffusivity, and stacking fault energy (using Fe as an example).

### 3.1 Computation of Interfacial Energy

The α/γ interfacial energy of Fe is a key physical quantity controlling nucleation and growth kinetics of α/γ phase transformations in steels. Experimental measurement of interfacial energy, especially its anisotropy (orientation dependency) is not trivial. Those quantities can be rather easily obtained by an atomistic computation. Figure 2(a)

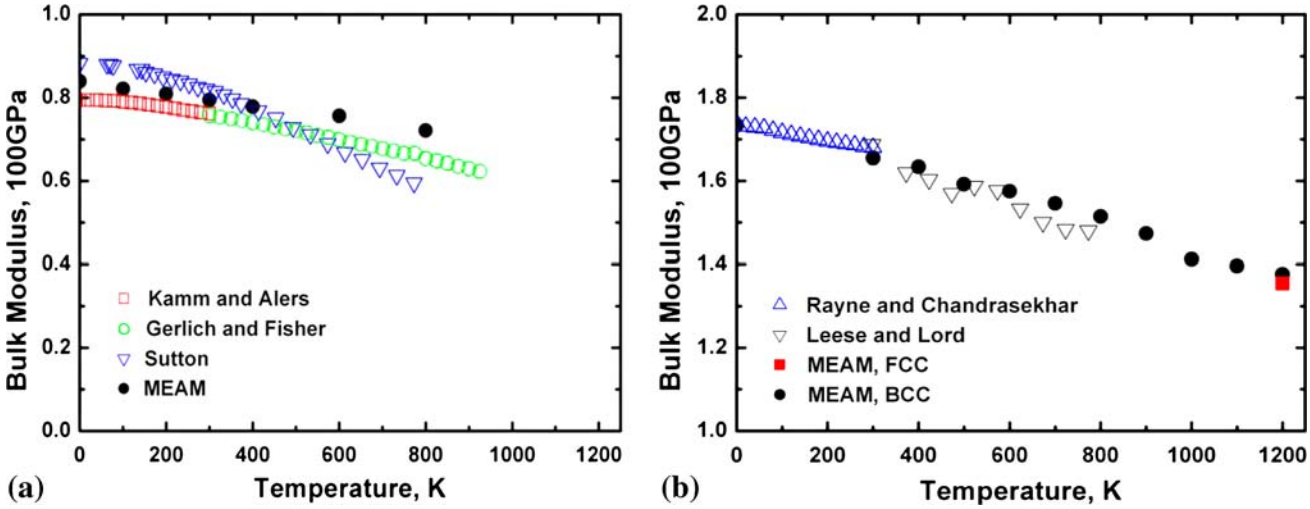


**Fig. 1** Calculated bulk modulus of (a) pure Al and (b) pure Fe according to the 2NN MEAM interatomic potentials,[5,6] in comparison with experimental data[22-26]

**Table 2 Physical properties of various structures in the Ni-W system calculated based on the MEAM potential,[15] in comparison with experimental data or FP calculation[27]**

| | *a*, Å | | | *c*, Å | | | $E_c$, eV | | *B*, GPa | |
|---|---|---|---|---|---|---|---|---|---|---|
| | Exp | FP | MEAM | Exp | FP | MEAM | FP | MEAM | FP | MEAM |
| $D1_a$ $Ni_4W$ | 5.73 | ··· | 5.73 | 3.553 | ··· | 3.553 | 5.40 | 5.36 | 293 | 292 |
| $L1_2$ $Ni_3W$ | ··· | 3.58 | 3.62 | ··· | ··· | 3.58 | 5.65 | 5.58 | 287 | 319 |
| $L1_2$ $NiW_3$ | ··· | 3.84 | 3.86 | ··· | ··· | 3.76 | 7.55 | 7.29 | 283 | 316 |
| $D0_{19}$ $Ni_3W$ | ··· | 2.53 | 2.56 | ··· | 4.05 | 4.15 | 5.42 | 5.59 | 289 | 316 |
| $D0_{19}$ $NiW_3$ | ··· | 2.76 | 2.76 | ··· | 4.44 | 4.38 | 7.70 | 7.36 | 304 | 321 |

and (b) shows two different superstructures composed of bcc and fcc Fe lattices with an interface according to the Kurdjumov-Sachs (K-S) relation and with variable interfaces. From the energy difference between the superstructure and individual lattices, the α/γ interfacial energy with the K-S relation and average interfacial energy of random interfaces can be calculated. The calculated K-S and Nishiyama-Wasserman interfacial energies are 0.33 and 0.32 J/m$^2$, respectively. The average value of random interfaces is calculated to be 1.08 J/m$^2$, which is comparable with experimental value of 0.80 J/m$^2$.[28] The ratio between the average interfacial energy and surface energy is about 0.4 which is also comparable with experimentally measured value of 0.38.[28] The grain boundary energies can also be calculated using similar methods.[29]

### 3.2 Computation of Grain Boundary Diffusivity

As the grain size decreases the role of grain boundaries in microstructural evolution becomes more and more decisive. One of the main grain boundary phenomena is fast diffusion or fast atomic mobility. Figure 3(a) shows the calculated self diffusivity of bcc Fe using the present MEAM potential,[5] showing a good agreement with experimental values.[30] By comparing the overall diffusivity in a single crystalline sample with that in a sample with a grain boundary, the grain boundary diffusivity can be estimated. The calculated grain boundary diffusivity of several types of grain boundaries is plotted in Fig. 3(b). Experimentally reported values[31] for the grain boundary diffusivity ($\delta D_{GB}$) in bcc Fe vary between $10^{-22}$ and $10^{-19}$ m$^3$/s in a temperature range of 700 to 1000 K. The calculated values in Fig. 3(b) are in good agreement with experimental data. According to the atomistic calculations, the ratio of the activation energy between grain boundary diffusion and bulk diffusion is around 20%, which is also in good agreement with experimental value of 22%.[31]

### 3.3 Computation of Stacking Fault Energy

Because of the strong correlation between stacking fault energy and deformation behavior of fcc metals, many efforts are being made to calculate the stacking fault energy and effects of alloying elements on it. Figure 4(a) shows the effect of Mn on the intrinsic stacking fault energy in fcc Fe[8] based on an atomistic calculation. Here, the stacking fault energy in pure fcc Fe is set to be zero. According to the present calculation, the stacking fault energy of fcc Fe decreases up to about 5 at.% Mn and then increases with increasing Mn content. Figure 4(b) shows the effect of Mn on the stacking fault energy in various austenitic steels obtained from experiments[32,33] or a thermodynamic calculation.[34] Even though there are differences in the absolute values between the present calculation and literature data and also among the literature data sets, all results show a qualitative agreement in that the stacking fault energy initially decreases with Mn addition and then increases with further addition of Mn. Similar calculations can be made for the effects of other alloying elements in higher order alloy systems.

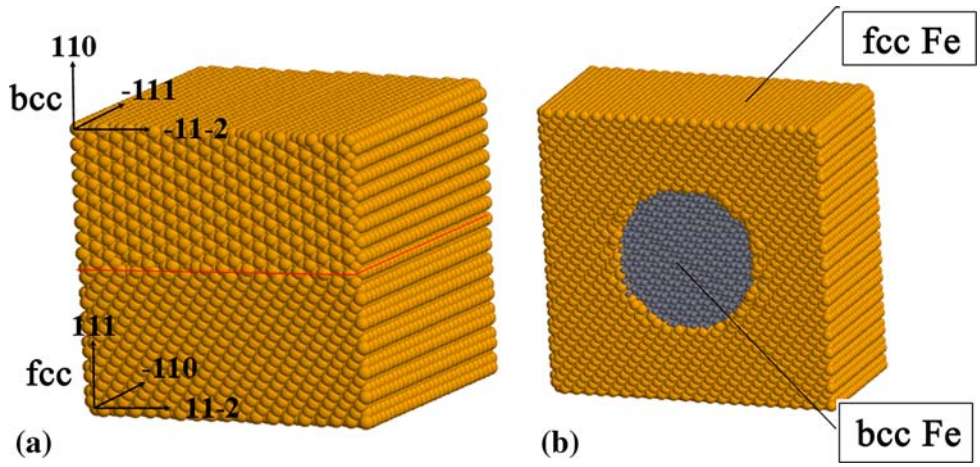


**Fig. 2** Superstructure composed of bcc and fcc Fe used for computation of (a) the K-S interfacial energy and (b) an average value of random interfaces

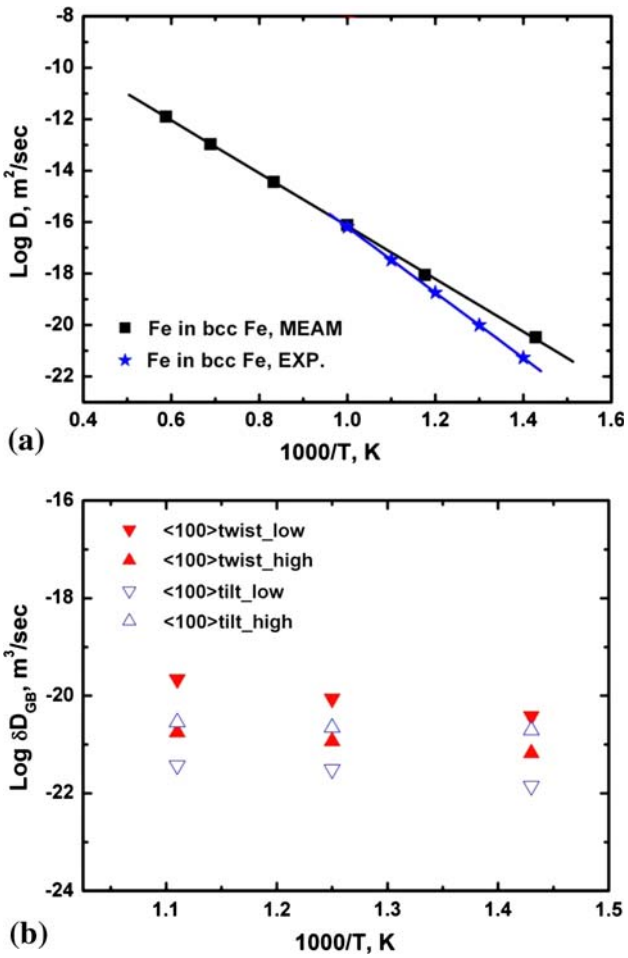


**Fig. 3** Calculated (a) self-diffusivity of bcc Fe in comparison with experimental data[30] and (b) grain boundary diffusivity on some grain boundaries in bcc Fe

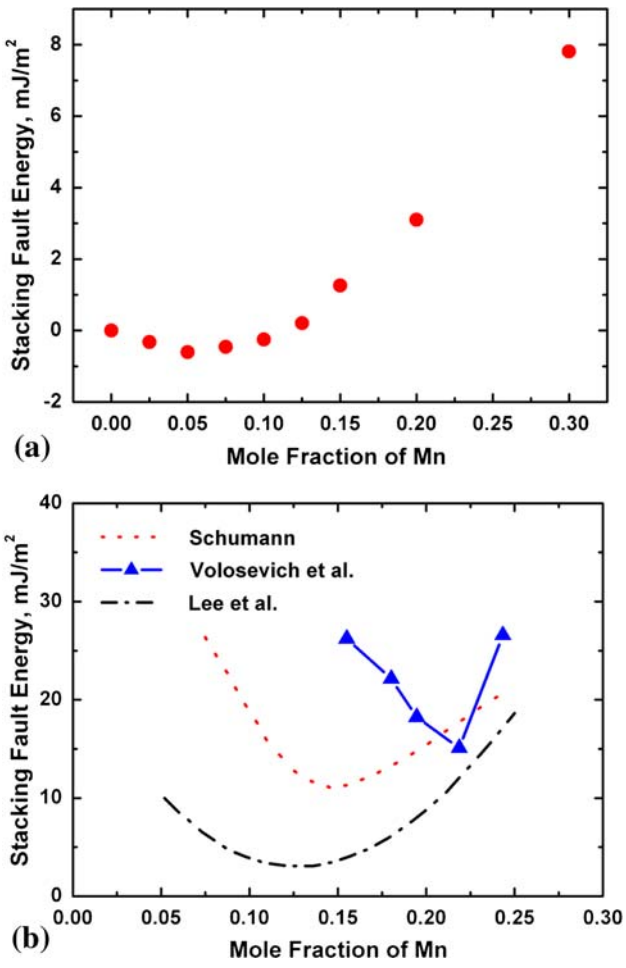


**Fig. 4** Effect of Mn on the intrinsic stacking fault energy of fcc Fe (a) by the present MEAM calculation,[8] and (b) by experiments[32,33] or thermodynamic calculation.[34] The stacking fault energy of pure Fe is set to be zero in (a)

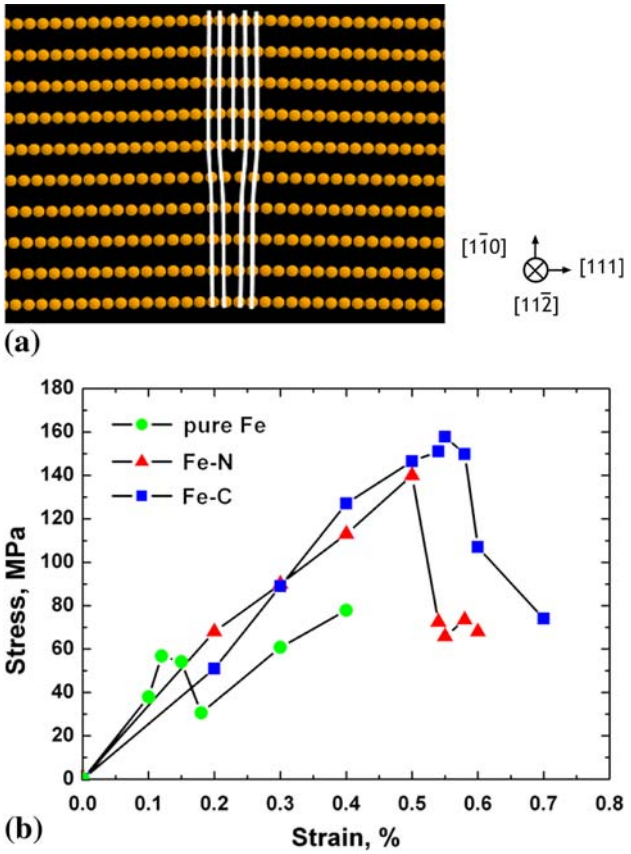


**Fig. 5** (a) A bcc Fe lattice with an edge dislocation and (b) resultant stress-strain curve of pure Fe and Fe with a C or N atom at 10 K based on atomistic simulation

## 4. Application of Atomistic Approaches

It is shown above that fundamental planar defect properties can be reasonably predicted by atomistic computations. The atomistic approach can be further applied to analyze fundamental material phenomena in both bulk and nanostructured materials.

### 4.1 Interactions Between Dislocations and Other Defects

The interactions between a dislocation and other defects (solute atoms, other dislocations, precipitates, grain boundaries, etc.) are key factors for estimating the mechanical properties from microstructures. As a first step of a multiscale simulation scheme to predict mechanical property of structural materials, calculations were performed on the critical resolved shear stress (CRSS) for the movement of an edge dislocation and effect of interstitial solute atoms on CRSS. Figure 5 shows a bcc Fe lattice with an edge dislocation, as an example, and the resultant stress-strain curve of pure Fe and Fe with a carbon or nitrogen atom at 10 K. Since the lattice structure was set in a way that the direction of burgers vector is parallel to the shear stress, the CRSS can be directly read from the flow stress. However, due to the unrealistically high strain rate given in the molecular dynamics simulation, the CRSS can always be overestimated by this simulation. The stress-strain curve in Fig. 5(b) shows a decrease of the flow stress after the onset of the yield point, and the lower bound of the flow stress should be regarded as the more realistic CRSS value rather than that at the yield point.

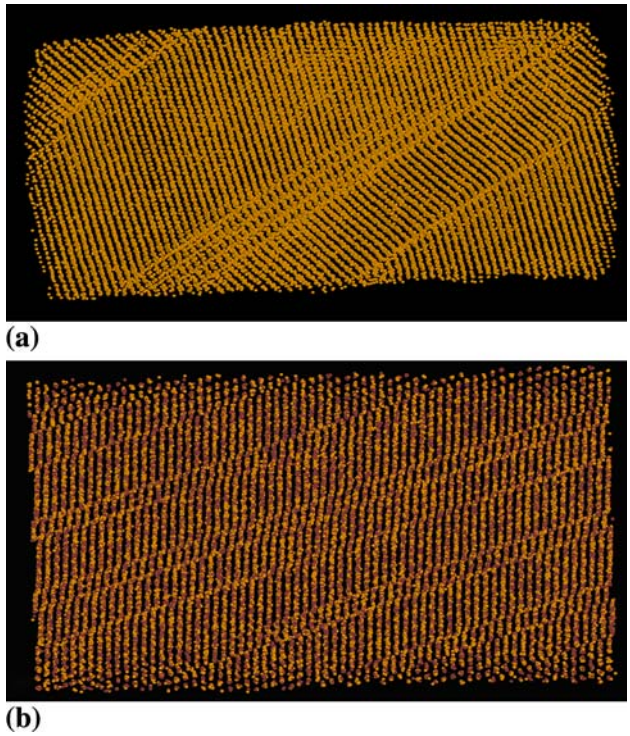


**Fig. 6** Plastic deformation in (a) fcc Fe (martensitic twinning) and (b) fcc Fe–40%Ni (slip) under uniaxial loading along $<111>$ direction at 300 K

### 4.2 Plastic Deformation

Various plastic deformation mechanisms operate depending on the magnitude of the stacking fault energy. The deformation mechanism in different materials systems and the variation of the mechanism according to crystallographic orientations can be effectively examined using molecular dynamics simulations. Figure 6 shows that the deformation in pure fcc Fe and fcc Fe-Ni alloys occurs differently (martensitic twinning versus slip). It looks reasonable to observe a deformation-induced martensitic transformation in fcc Fe at room temperature and a slip in an fcc alloy stabilized by adding an austenite-forming element, Ni. Using these simulations on a wide range of alloys, the effect of alloying elements on the deformation behavior of structural metallic alloys and the probable correlation between the magnitude of stacking fault energy and the deformation mechanism can be investigated.

### 4.3 Thermodynamics of Nanoparticles

With advances in technology, the size of devices and device materials are getting down to nanometer scale. Various fundamental physical properties are expected to

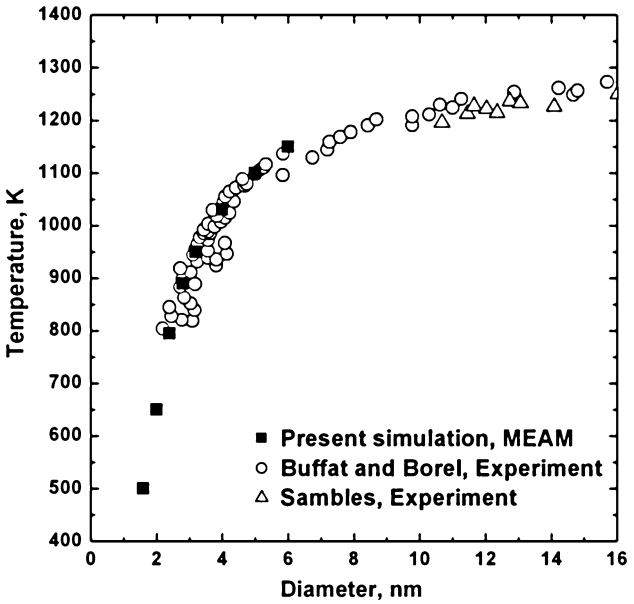


**Fig. 7** Melting temperature of pure gold nanoparticle as a function of particle diameter,[35] in comparison with experimental data[36,37]

change as the size decreases. A typical example of the size dependency of physical properties is melting point depression. Figure 7 shows that the melting point depression of Au nanoparticles is correctly reproduced by a molecular dynamics simulation.[35] In addition to the melting point of pure elements, all possible size effects on thermodynamic properties of alloys and compounds can be investigated using the atomistic approaches.

### 4.4 Atomistic Distribution in Alloy Nanowires

The chemical composition of $Si_{1-x}Ge_x$ nanowires determines its electronic characteristics, thus it is regarded as one of critical factors controlling advanced device performance. Understanding the effects of various process conditions on the atomic configuration in $Si_{1-x}Ge_x$ nanowires is essential for fine tuning materials properties. Figure 8 shows a simulated atomic configuration and composition profiles in the radial direction of $Si_{1-x}Ge_x$ nanowires at various thermodynamic process conditions (chemical potential difference between Si and Ge). The size dependency of the alloy nanowire composition recently found and rationalized[38] can also be investigated in more detail by the atomistic simulations.

### 4.5 Local Stress and Strain Distribution Around a Quantum Dot

The misfit stress around a quantum dot (QD) plays a decisive role in the evolution of the shape and vertical alignment of the QDs, and it also has a significant effect on the energy band gap of the QD during and after their formation. Analysis of the local stress distribution around a QD is therefore essential for successful fabrication of QD

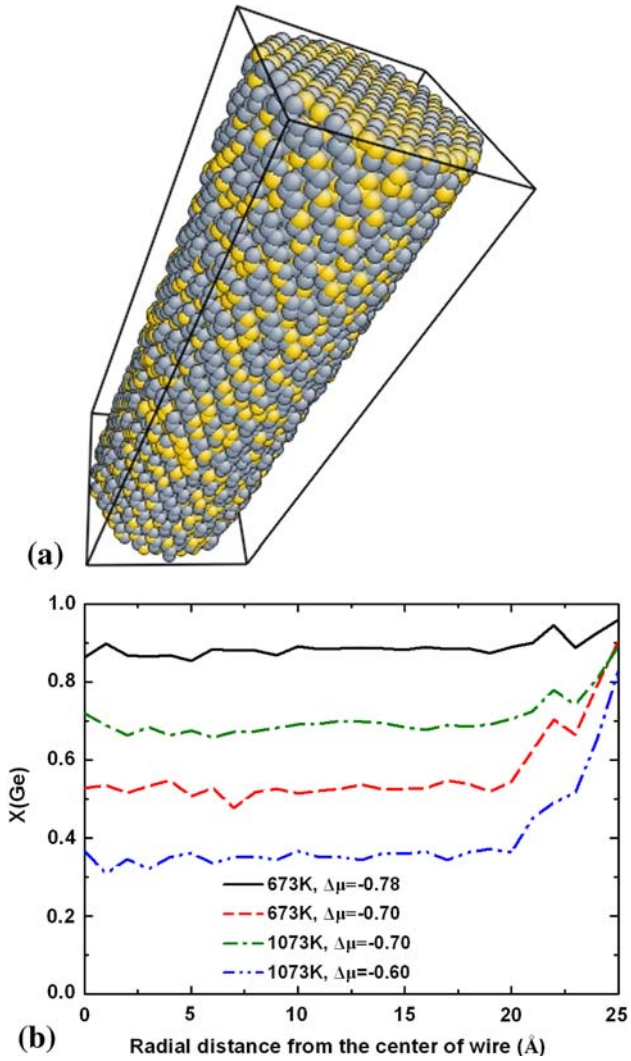


**Fig. 8** (a) A simulated atomic configuration and (b) composition profiles in the radial direction of $Si_{1-x}Ge_x$ nanowires at various thermodynamic process conditions. Δμ is the chemical potential difference between Si and Ge (eV)

structures. Figure 9 shows the calculated local strain distribution in the vertical section at the center of a InAs/GaAs QD system.[39] On the left is the distribution of the hydrostatic component. The different gray scales represent the state of the strain (tensile or compressive). On the right, the planar and vertical components, as well as the hydrostatic component along the vertical line at the center of the QD, are plotted as a function of distance from the substrate. Both the hydrostatic strain and stress are shown to propagate up to about 160 Å from the substrate. The corresponding experimental value is about 150 Å.[40] The good agreement in the range of the local strain between the experimental and calculation results indicates the reliability of the MEAM interatomic potential and the applicability of the atomistic approaches to the design and control of morphological evolution in nanostructures.

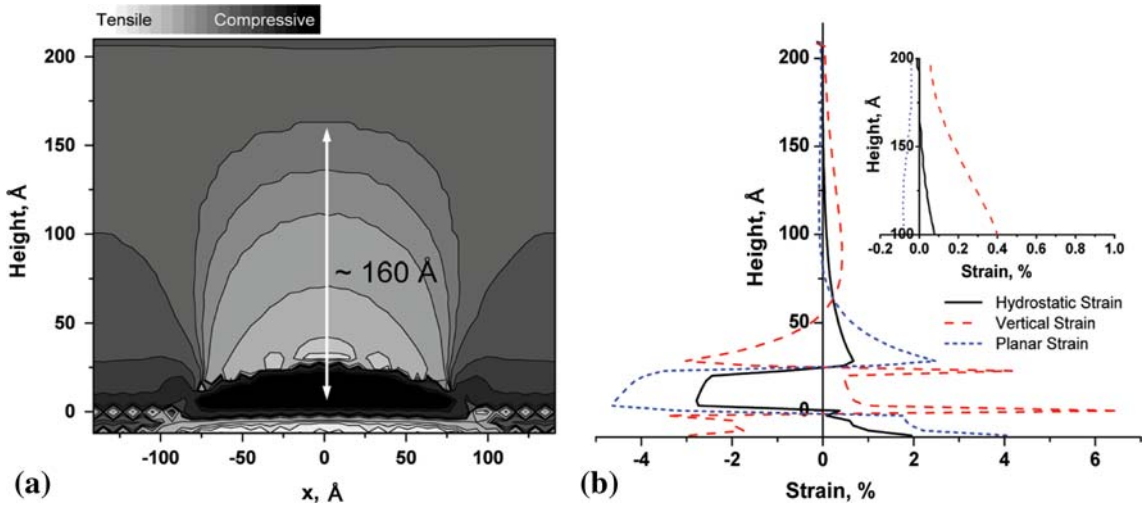


**Fig. 9** Hydrostatic strain distribution around an InAs QD embedded between a GaAs substrate and a capping layer.[39] The vertical and planar components of the strain/stress are plotted on the right

## 5. Summary

The examples of this article show that atomistic simulation techniques based on the 2NN MEAM interatomic potentials can be utilized to provide fundamental physical properties (interface or grain boundary energy, diffusivity, and stacking fault energy) necessary for advanced materials and process design and also to analyze various materials phenomena in both bulk and nanostructured materials.

### Acknowledgments

This work was financially supported by the Ministry of Knowledge Economy of Korea and the Pohang Steel Company (POSCO).

### References

1. A.E. Carlsson, *Solid State Physics: Advances in Research and Application*, Vol 43, H. Ehrenreich and D. Turnbull, Ed., Academic Press, New York, 1990,
2. M.I. Baskes, Modified Embedded-Atom Method Potentials for Cubic Materials and Impurities, *Phys. Rev. B*, 1992, **46**, p 2727-2742
3. M.S. Daw and M.I. Baskes, Embedded-Atom Method: Derivation and Application to Impurities, Surfaces, and Other Defects in Metals, *Phys. Rev. B*, 1984, **29**, p 6443-6453
4. B.-J. Lee and M.I. Baskes, Second Nearest-Neighbor Modified Embedded-Atom Method Potential, *Phys. Rev. B*, 2000, **62**, p 8564-8567
5. B.-J. Lee, M.I. Baskes, H. Kim, and Y.K. Cho, Second Nearest-Neighbor Modified Embedded Atom Method Potentials for BCC Transition Metals, *Phys. Rev. B*, 2001, **64**, p 184102:1-184102:10
6. B.-J. Lee, J.-H. Shim, and M.I. Baskes, Semi-Empirical Atomic Potentials for the FCC Metals Cu, Ag, Au, Ni, Pd, Pt, Al and Pb Based on First and Second Nearest-Neighbor Modified Embedded Atom Method, *Phys. Rev. B*, 2003, **68**, p 144112:1-144112:11
7. Y.-M. Kim, B.-J. Lee, and M.I. Baskes, Modified Embedded Atom Method Interatomic Potentials for Ti and Zr, *Phys. Rev. B*, 2006, **74**, p 014101:1-014101:12
8. Y.-M. Kim, Y.-H. Shin, and B.-J. Lee, Modified Embedded-Atom Method Interatomic Potentials for Pure Mn and Fe-Mn System, *Acta Mater.*, 2009, **57**, p 474-482
9. B.-J. Lee and J.W. Lee, A Modified Embedded Atom Method Interatomic Potential for Carbon, *CALPHAD*, 2005, **29**, p 7-16
10. B.-J. Lee, A Modified Embedded Atom Method Interatomic Potential for Silicon, *CALPHAD*, 2007, **31**, p 95-104
11. E.H. Kim, Y.-H. Shin, and B.-J. Lee, A Modified Embedded Atom Method Interatomic Potential for Germanium, *CALPHAD*, 2008, **32**, p 34-42
12. B.-J. Lee, B.D. Wirth, J.-H. Shim, J. Kwon, S.C. Kwon, and J.-H. Hong, An MEAM Interatomic Potential for the Fe-Cu Alloy System, Cascade Simulation on Pure Fe, Fe-Cu Alloy, *Phys. Rev. B*, 2005, **71**, p 184205:15-184205:15
13. J. Kim, Y. Koo, and B.-J. Lee, Modified Embedded-Atom Method Interatomic Potential for the Fe-Pt Alloy System, *J. Mater. Res.*, 2006, **21**, p 199-208
14. I. Sa and B.-J. Lee, Modified Embedded-Atom Method Interatomic Potentials for the Fe-Nb and Fe-Ti Systems, *Scripta Mater.*, 2008, **59**, p 595-598
15. J.-H. Shim, S.I. Park, Y.W. Cho, and B.-J. Lee, Modified Embedded-Atom Method Calculation for the Ni-W System, *J. Mater. Res.*, 2003, **18**, p 1863-1867
16. B.-J. Lee, A Modified Embedded Atom Method Interatomic Potential for the Fe-C System, *Acta Mater.*, 2006, **54**, p 701-711
17. B.-J. Lee, T.-H. Lee, and S.-J. Kim, A Modified Embedded-Atom Method Interatomic Potential for the Fe-N System: A Comparative Study with the Fe-C system, *Acta Mater.*, 2006, **54**, p 4597-4607
18. B.-J. Lee and J.-W. Jang, A Modified Embedded-Atom Method Interatomic Potential for the Fe-H System, *Acta Mater.*, 2007, **55**, p 6779-6788
19. Y.-M. Kim and B.-J. Lee, Modified Embedded-Atom Method Interatomic Potentials for the Ti-C and Ti-N Systems, *Acta Mater.*, 2008, **56**, p 3481-3489

20. J.H. Rose, J.R. Smith, F. Guinea, and J. Ferrante, Universal Features of the Equation of State of Metals, *Phys. Rev. B*, 1984, **29**, p 2963-2969
21. M.I. Baskes, Determination of Modified Embedded Atom Method Parameters for Nickel, *Mater. Chem. Phys.*, 1997, **50**, p 152-158
22. G.N. Kamm and G.A. Alers, Low-Temperature Elastic Moduli of Aluminum, *J. Appl. Phys.*, 1964, **35**, p 327-330
23. D. Gerlich and E.S. Fisher, The High Temperature Elastic Moduli of Aluminum, *J. Phys. Chem. Solids*, 1969, **30**, p 1197-1205
24. P.M. Sutton, The Variation of the Elastic Constants of Crystalline Aluminum with Temperature between 63 K and 773 K, *Phys. Rev.*, 1953, **91**, p 816-821
25. B.S. Chandrasekhar and J.A. Rayne, Elastic Constants of Indium From 1.4 to 300 K, *Phys. Rev.*, 1961, **124**, p 1011-1014
26. J. Leese and A.E. Lord, Elastic Stiffness Coefficients of Single-Crystal Iron from Room Temperature to 500°C, *J. Appl. Phys.*, 1968, **39**, p 3986-3988
27. L.T. Kong, J.B. Liu, W.S. Lai, and B.X. Liu, Correlation of Lattice Constant Versus Tungsten Concentration of the Ni-based Solid Solution Examined by Molecular Dynamics Simulation, *J. Alloys Compd.*, 2002, **337**, p 143-147
28. Z. Yang and R.A. Johnson, An EAM Simulation of the $\alpha$-$\gamma$ Iron Interface, *Model. Simul. Mater. Sci. Eng.*, 1993, **1**, p 707-716
29. B.-J. Lee and S.-H. Choi, Computation of Grain Boundary Energies, *Model. Simul. Mater. Sci. Eng.*, 2004, **12**, p 621-632
30. H. Bester and K.W. Lange, Estimation of Average Values for the Diffusion of C, $O_2$, $H_2$, $N_2$ and S in Solid and Liquid Iron, *Arch. Eisenhuttenwes.*, 1972, **43**, p 207-213
31. A. Inoue, H. Nitta, and Y. Iijima, Grain Boundary Self-Diffusion in High Purity Iron, *Acta Mater.*, 2007, **55**, p 5910-5916
32. H. Schumann, Einfluß der Stapelfehlerenergie auf den Kristallographischen Umgitterungsmechanismus der Gamma/Alpha-Umwandlung in Hochlegierten Stählen, *Krist. Tech.*, 1974, **9**, p 1141-1152
33. P.Yu. Volosevich, V.N. Grindnev, and Y.N. Petrov, Manganese Influence on Stacking-Fault Energy in Iron-Manganese Alloys, *Phys. Met. Metallogr.*, 1976, **42**, p 126-130
34. Y.-K. Lee and C.-S. Choi, Driving Force for $\gamma \rightarrow \varepsilon$ Martensitic Transformation and Stacking Fault Energy of $\gamma$ in Fe-Mn Binary System, *Metall. Mater. Trans. A*, 2000, **31**, p 355-360
35. J.-H. Shim, B.-J. Lee, and Y.W. Cho, Thermal Stability of Unsupported Gold Nanoparticle: A Molecular Dynamics Study, *Surf. Sci.*, 2002, **512**, p 262-268
36. Ph. Buffat and J.-P. Borel, Size Effect on the Melting Temperature of Gold Particles, *Phys. Rev. A*, 1976, **13**, p 2287-2298
37. J.R. Sambles, An Electron Microscope Study of Evaporating Gold Particles: The Kelvin Equation for Liquid Gold and the Lowering of the Melting Point of Solid Gold Particles, *Proc. R. Soc. Lond. A*, 1971, **324**, p 339-351
38. I. Sa, B.-M. Lee, C.-J. Kim, M.-H. Jo, and B.-J. Lee, Thermodynamic Analysis for the Size-Dependence of Si1-x-Gex Nanowire Composition Grown by a Vapor-Liquid-Solid Method, *CALPHAD*, 2008, **32**, p 669-674
39. E.C. Do and B.-J. Lee, Atomistic Computation of Local Stress and Strain Distribution Around an InAs Quantum Dot Between a GaAs Capping Layer and a Substrate, *Electron. Mater. Lett.*, 2008, **4**, p 107-111
40. H.S. Kim, J.H. Suh, C.G. Park, S.J. Lee, S.K. Noh, J.D. Song, Y.J. Park, W.J. Choi, and J.I. Lee, Structure and Strain Characteristics of Self-Assembled InAs/GaAs Quantum Dots Investigated by Transmission Electron Microscopy, *J. Korean Inst. Met. Mater.*, 2006, **44**, p 518-526